Journal of Materials Chemistry A

REVIEW

View Article Online
View Journal | View Issue

Cite this: J. Mater. Chem. A, 2023, 11, 5408

3D direct ink printed materials for chemical conversion and environmental remediation applications: a review

Jeannie Z. Y. Tan, *[ab] Manuel Alejandro Ávila-López, [c] Amir Jahanbakhsh, [ab] Xuesong Lu,†[a] José Bonilla-Cruz, [c] Tania E. Lara-Ceniceros, *[c] John M. Andresen [ab] and M. Mercedes Maroto-Valer *[ab]

Received 15th November 2022
Accepted 11th February 2023

DOI: 10.1039/d2ta08922j

rsc.li/materials-a

3D printing technologies and continuous flow microreaction systems are rapidly gaining attention in the domain of heterogeneous catalysis. From a materials perspective, minimising material waste through simplified single (or few) step fabrication processes is attractive for commercial exploitation. Direct ink writing (DIW) has recently studied as potential printing technology for energy storage, such as batteries and capacitors. However, the use of DIW to develop catalysts and microreactors for photo-, photoelectro-, and electrocatalysis reactions for chemical conversion and environmental remediation applications has not been developed as much as reported for energy storage applications. Hence, this review summarises the most recent development of DIW for photo-, photoelectro-, and electrocatalysis

[a]Research Centre for Carbon Solutions (RCCS), School of Engineering & Physical Sciences, Institute of Mechanical, Process & Energy Engineering, Heriot-Watt University, Edinburgh EH14 4AS, UK. E-mail: M.Maroto-Valer@hw.ac.uk

[b]Industrial Decarbonisation Research and Innovation Centre (IDRIC), Heriot-Watt University, Edinburgh EH14 4AS, UK

[c]Nano & Micro Additive Manufacturing of Polymers and Composite Materials Laboratory "3D LAB", Advanced Functional Materials & Nanotechnology Group, Centro de Investigación en Materiales Avanzados S. C. (CIMAV-Subsede Monterrey), C. P. 66628 Apodaca, Nuevo León, Mexico. E-mail: tania.lara@cimav.edu.mx

† Current address: Department of Chemical and Biological Engineering, University of Sheffield, Mappin Street, Sheffield, S1 3JD, United Kingdom.

Dr Jeannie Z. Y. Tan (MRSC) is currently a research fellow of the Research Centre for Carbon Solutions (RCCS) and project technical lead of the UK Industrial Decarbonisation Research and Innovation Centre (IDRIC). She received her BSc (2010) from The Universiti Sains Malaysia, and her Msc (2013) from Zhejiang University. She obtained her PhD (2017) from The University of Melbourne and after that joined the RCCS at Heriot–Watt University as Research Associate. She currently has 34 publications that have been cited over 1000 times and a book chapter. She was received the IAAM Young Scientist Medal in recognition of her contribution to Micro and Nanostructured Materials.

Dr Manuel Alejandro Ávila López is member of the National Investigation System (SNI candidate). He received his BSc (2015), MSc (2018) and PhD (2021), from the Autonomous University of Nuevo León (UANL). His background is working on developing scalable and low-cost photocatalyst materials films and coatings for CO_2 photocatalytic reduction in liquid and gas phase under visible light and the development of CO_2 capture materials based on semiconductor material powders and coatings. Since June 2021 is working as Postdoctoral Fellow at Research Center for Advanced Materials (CIMAV, S. C.-Monterrey Campus), Advanced Functional Materials & Nanotechnology Group, and Nano & Micro Additive Manufacturing of Polymers and Composite Materials Laboratory, 3D LAB. He is developing scalable, and low-cost 3D printed photocatalyst materials via *direct ink writing, robocasting, and Stereolithography. He currently has 10 publications that have been cited 50 times.*

reactions for chemical conversion and environmental remediation applications. Recent trends, such as fast prototyping of reactors *via* 3-D printing of flow channels, miniaturisation and use of multi-physics modelling, are also highlighted. Finally, a perspective of DIW development to accurately fabricate nanostructured catalysts as well as reactions for catalytic applications is presented.

1. Introduction

To preserve a liveable climate, greenhouse-gas emissions must be reduced to net zero by 2050.[1] Hence, the development of clean energy plays an important role to tackle the climate emergency and build a sustainable world by driving the industry to decarbonized chemical manufacturing as well as remedy environmental issues. However, the commercialization of clean energy systems requires a significant improvement in their performance and efficiency.

According to the definition standardised by Technical Committee of the American Society for Testing and Materials (ASTM) International in NF ISO/ASTM 52900, additive manufacturing (AM) is the process of joining materials to make objects from 3D model data, usually layer upon layer, as opposed to subtractive manufacturing methodologies.[2] Unlike subtractive manufacturing processes, AM can directly produce complex 3D parts, with near-complete design freedom. Hence, it is advantageous products that have a high demand of customization, flexibility, design complexity and high transportation costs. It shows a great potential towards manufacturing novel designs of energy conversion and storage devices, which were previously inaccessible *via* traditional manufacturing methods. Other advantages of AM include reduced lead time and it is a more sustainable manufacturing technology as there is virtually no waste material. Extended discussions on the details and capabilities of a range of 3D printing methods can be found in recently published review articles.[3–9]

Catalysis is a driving force of the chemical industry. To intensify catalytic processes to make them more efficient and sustainable, the growth of AM for catalysis applications is growing exponentially with a myriad of strategies to obtain devices with catalytic properties. For example, a few studies and reviews have discussed the advantages and implications of 3D (three-dimensional) printed devices and materials for electrochemical energy storage[6–8,10,11] and environmental remediation applications.[12,13] Well-designed 3D structures were reported to have great potentials for increasing the performance of batteries, capacitors, fuel cells and advanced photovoltaic cells,[14] as well as leading to improvements in reactor engineering and catalysis applications.[15–17] For instance, by combining absorbers and reflectors with self-supporting 3D photovoltaic (3DPV) structures, which were achieved by mounting commercial Si cells on AM fabricated 3D plastic frames, the energy densities yielded were reported to be higher by a factor of 2–20 than stationary flat PV panels, compared to the increase by a factor of 1.3–18 for a flat panel with dual-axis

Dr Amir Jahanbakhsh is a Research Fellow and Programme manager of the Research Centre for Carbon Solutions (RCCS) at Heriot–Watt University. Amir has a PhD in Petroleum Engineering from Heriot–Watt University and he is also an experienced project manager. His research focus is on the understanding of the multiphase flow mechanisms in porous media at different scales using various techniques including CFD and microfluidics. Carbon capture and storage, geo-energy and more recently hydrogen economy have been his main area of research. Since he joined RCCS he has been involved in managing large multidisciplinary consortium projects including an ERC-funded project – MILEPOST-Microscale Processes Governing Global Sustainability, two EPSRC-funded projects – low carbon jet fuel through integration of novel technologies for co-valorisation of CO_2 and biomass and novel adsorbents applied to integrated energy-efficient industrial CO_2 capture and one ERA–ACT funded project- PrISMa (Process-Informed design of tailor-made Sorbent Materials for energy efficient carbon capture).

Dr Xuesong Lu is currently a research associate in Department of Chemical and Biological Engineering, University of Sheffield. He received his Bachelor degree from Beijing University of Chemical Technology in 1993 and his Master degree from Northwest University, Xi'an in 1996. He obtained his PhD degrees from Institute of Process Engineering, Chinese Academy of Sciences in 2000 and Cambridge University in 2017. During the period of 2020 to 2021, he worked as a research associate at the Research Centre for Carbon Solutions (RCCS), Heriot–Watt University. He currently has more than 70 publications that have been cited over 1500 times.

sun tracking.[18] AM can also be utilized during fabrication of microstructures that are capable of increasing the efficiency of single-junction solar cells.[19–21]

3D printing for photo-, electro-, and photo(electro)-chemical energy conversion and storage application is relatively new, only gaining momentum in the research world recently.[5,6,22] To enable improvements in resource efficiency as well as in sustainable production and consumption, Gebler *et al.* suggested that replacing conventional manufacturing with AM has the potential to reduce total energy primary supply (TEPS) by 2.54–9.30 EJ and CO_2 emissions by 130–525.5 Mt over its entire life-cycle.[23] This implies that AM can transform the manufacturing system. Hence, AM is an attractive alternative to traditional subtractive fabrication techniques because it can rapidly produce cost effective and complex prototypes with varying degrees of functionality. Parts produced by AM have found applications in industries, such as aerospace,[24] defense,[25] construction,[26] and biomedical.[27,28]

AM also termed 3D printing, has become a major driver of innovation in industrial manufacturing today.[29,30] Today, 3D printing has become a fabrication tool for final products in addition to prototyping. The principles of AM have been explained in detail in numerous public articles.[31,32] According to ASTM F2792-12a, 3D printing techniques can be categorised based on the printing methods, such as material extrusion (*i.e.*, direct ink writing – DIW) and fused deposition modelling (FDM), powder bed fusion (*i.e.*, selective laser sintering – SLS and direct metal laser sintering), vat photopolymerization (*i.e.*, stereolithography – SLA), binder jetting, material jetting (*i.e.*, inkjet printing – IJP), sheet laminate (*i.e.*, laminated object manufacturing – LOM) and directed energy deposition.[33] Overall, compared with the conventional subtractive methods, 3D printing provides a completely new bottom-up manufacturing technology to rapidly fabricate 3D-structured devices with complex architecture of materials, minimal waste and low cost.

Dr José Bonilla Cruz is currently a Titular Researcher at the Research Center for Advanced Materials (CIMAV-Monterrey Campus) since 2008. He received a BSc degree from The Instituto Tecnológico de Veracruz (1998) and MSc degree from Instituto Tecnológico de Celaya (2002), both in Chemical Engineering. He worked in the Polymer industry as Jr Researcher (2001–2004) at the Research Center and Technological Development (CID, DESC-Group). He obtained his Doctoral degree in Polymer Science with honors (2008). In 2019 he took a Sabbatical stay in CWRU about 3D printing of polymeric materials with Prof. Rigoberto Advíncula. His research interests are in the areas of functional polymers synthesis, covalent functionalization of graphene oxide and its polymer composites, as well 3D printing of polymers and composite materials for Advanced Applications in Sensing, Super-Anticorrosive, Supercapacitors, Photocatalyst, CO_2 Capture/reaction, among others. He is leading the Nano & Micro Additive Manufacturing of Polymers and Composite Materials Laboratory "3D LAB" at CIMAV. He is recognized as member of the National Researcher System (Level 1) from CONACYT-México. He currently has 46 publications, and 2 book chapters that have been cited over 600 times. Also, he has been chairman and organizer of several national and international meetings of Polymer Science (MACROMEX, Biannual US-Mexico meeting; PPC, polymer pacific conference, among others).

Dr Tania E. Lara Ceniceros is currently a Titular Researcher at Research Center for Advanced Materials (CIMAV, S. C.-Monterrey Campus). She received her BSc. in Chemistry-Specialty in Organic Chemistry from the Autonomous University of Coahuila (2002). She earned her PhD in Polymer Science and Technology from CIQA (Research Center for Applied Chemistry) (2008). She is an established researcher in polymer science and nanotechnology with focus on synthesis and characterization of nanomaterials and their functionalization for advanced applications including photodegradation for water remediation towards emergent pollutants and heavy metals. She holds the recognition of National Researcher Level 1 from CONACYT-México. After her sabbatical leave as Visiting Researcher at Case Western Reserve University–Department of Macromolecular Science & Engineering (2019–2020) is driving the 3D and 4D printing of hydrocolloids, nanocellulose gels, and the design of photopolymerizable resins, inks and bioinks for Direct Ink Writing. Since her incorporation to CIMAV in 2009, she has 13 years of experience in courses in consolidated postgraduate programs in advanced materials and nanotechnology. She has led projects of technological importance in relevant areas such as paints, paper industry (cellulose industry), pharmaceutical, and chemical industry. She currently has 36 publications in international journals, including 3 book chapters which have been cited over 550 times. Since 2020, jointly with Dr José Bonilla leads the Nano & Micro Additive Manufacturing of Polymers and Composite Materials Laboratory "3D LAB" at CIMAV. Current President of the Polymer Society of Mexico SPM (2021–2023).

Among the printing techniques, FDM, DIW, SLA, LOM, and SLS are widely used techniques for catalyst preparation[34] because they are capable to reach down to micro- and nano-scale structures.[17]

2. Direct ink writing (DIW) technology

Among the various AM techniques, DIW has emerged as the most versatile 3D printing technique for the broadest range of

Prof. John M. Andresen is a Professor in Energy Systems at Heriot–Watt University and Associate Director of Low-Carbon Systems within the Research Centre for Carbon Solutions. His main expertise involves systems integration and decarbonisation opportunities, sustainable fuels, optimisation of combined energy and water savings and life cycle analysis (LCA). He is the ETP Hydrogen Strategic Champion, member of the RSB Power-to-X Working Group and sits on the IEA Hydrogen TCP task force on Underground Hydrogen Storage. Dr Andresen has close to 100 publications spanning a range of energy intensive sectors. He has been active securing over £42m funding in the area of decarbonisation, particularly towards utilisation of industrial CO_2 back to chemicals and fuels (EP/N009924/1), aviation (EP/P015379/1), carbon footprint calculations (EP/P015379/1) and circular economy aspect of biomanufacturing (EP/W018969/1). Lately he became the CI of the £20m Industrial Decarbonisation Research and Innovation Centre (IDRIC, EP/V027050/1) with particular emphasis on synthetic fuels for decarbonisation.

Prof. M. Mercedes Maroto-Valer (FRSE, FIChemE, FRSC, FRSA, FEI) is Champion and Director of the UK Industrial Decarbonisation Research and Innovation Centre (IDRIC) that forms part of the UK Industrial Decarbonisation Challenge focused on accelerating the transition to net zero of industrial clusters and establishing the first world net-zero industrial cluster. Prof. Maroto-Valer is Deputy Principal (Global Sustainability) at Heriot–Watt University, leading institutional and global changes in sustainability, making a significant impact on achieving the United Nations Sustainable Development Goals (SDGs) and working with partners to achieve global carbon reduction targets through the development of university wide initiatives (UK, Dubai and Malaysia). She is director of the Research Centre for Carbon Solutions (RCCS) at Heriot–Watt University, where she holds the Robert Buchan Chair in Sustainable Energy Engineering. RCCS is a world leading multidisciplinary centre delivering innovation for the wider deployment of low-carbon energy systems required for meeting net-zero targets. Her internationally recognised track record covers energy systems, CCUS, integration of hydrogen technologies and low carbon fuels. She has held academic appointments at the University of Kentucky (1997–1998), Pennsylvania State University (1998–2004) and University of Nottingham (2005–2012). She joined Heriot–Watt University in 2012 as the first Robert Buchan Chair in Sustainable Engineering and has been Director of the cross-university Energy Academy and Head of the Institute of Mechanical, Process and Energy Engineering, Assistant Deputy Principal (Research and Innovation) and Associate Principal (Global Sustainability). She has over 550 publications and has received numerous international prizes and awards, including 2021 ACES-Margarita Salas Prize, 2021 Disruptors + Innovators Best Research Project Prize, 2019 Scottish Women Award-Services to Science and Technology, 2019 Honorary Doctorate TU Delft, 2018 SRUK/CERU Merit Award, 2013 Hong-Kong University Mong Distinguished Fellowship, 2011 RSC ESED Early Career Award, 2009 Philip Leverhulme Prize, 2005 US Dep. of Energy Award for Innovative Development, 1997 Ritchie Prize, 1996 Glenn Award-Fuel Chemistry American Chem. Soc., 1993 ICI Chemical & Polymers Group Andersonian Centenary Prize. Her portfolio includes a prestigious European Research Council (ERC) Advanced Award. Prof. Maroto-Valer holds leading positions in professional societies/editorial boards, including her role in the Council of Engineers for the Energy Transition (CEET) under the auspices of the United Nations Secretary-General.

Table 1 Comparison of drop-on-demand inkjet and extrusion printing

Printing technique	Drop-on-demand inkjet printing	Extrusion printing
Characteristic	Generate individual droplets when required onto a substrate	Extension of conventional inkjet printing technology and can be used as a substrate-friendly method
Advantages	More economic in ink delivery	Highly versatile as a large variety of materials can be deposited
	High printing resolution as dilute suspensions are used	Higher density of material deposited
		Capable of forming 3D structure
Disadvantages	Printing only 2D direction	Complicated post printing process (*i.e.*, surfactant removal and post thermal annealing steps)
		Low feature resolution

materials. DIW allows printing of practically any material, provided the precursor ink can be engineered to demonstrate appropriate rheological behaviour.[35] The fabrication of catalytic materials for chemical conversion and environmental remediation applications using DIW is increasing gaining researchers' interest because this technique acts as a unique pathway to introduce design freedom, multifunctionality, and stability simultaneously into its printed structures.

2.1 Tools

DIW has gained extensive attention, as it shows superiority due to free choices of materials, small amount of raw materials, open source and feasibility for multi-material printing.[36,37] DIW is also called, robocasting, robot-assisted shape deposition, robotic deposition or 3D fibre deposition, and is a method associated with the material extrusion technique.[38] It was initially established by Cesarani *et al.* at Sandia National Laboratories in 1997 for the fabrication of concentrated materials, such as ceramic pastes with some portion of organic binder. This technique is an easy, adaptable, and inexpensive methodology, appropriate for a broad range of materials, such as ceramic materials (monolithic and composites), polymers, alloys, and even food.[39] It particular, DIW enables complex catalytic systems to be manufactured where traditional routes are not able to achieve the complexity of AM.

The DIW AM technique can be categorized by the two main manufacturing approaches:

(1) Discontinuous droplet-based (also known as drop-on-demand inkjet printing, Fig. 1a.

• Printing heads eject discontinuous droplets onto the printing substrate to produce the image by means of the heat-induced explosion of ink bubbles (*e.g.*, in bubble jet printers and thermal inkjets).[40]

(2) Continuous paste-based/filamentary ink approaches (Fig. 1b).[36]

• Pressurized ink is forced through a nozzle, and breaks up into uniform drops under the action of surface tension.[41]

The comparison of these two techniques is summarised in Table 1.

Recent studies have reviewed the recent progress of inkjet printing.[42–45] Furthermore, the ability of extrusion printing to fabricate self-standing 3D microstructure has received

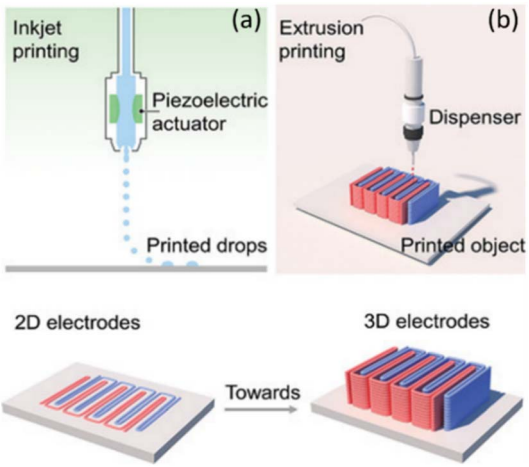

Fig. 1 Direct writing: (a) drop-on-demand inkjet printing wherein the ink is jetted onto a support in droplet form and (b) extrusion 3D-printing wherein the ink has a paste-like consistency for printing self-supporting structures (reprinted with permission from ref. 42).

widespread attention because this resolves the adhesion concern between the printed materials and substrate and the compatibility of substrate for post printing treatment (*e.g.*, post annealing step).[45–47] In addition, self-standing 3D printed catalysts ease the catalyst recovery process. Hence, the following discussion will focus on extrusion-based printing. The extrusion-based DIW utilizes a non-Newtonian viscous slurry with composed rheological properties (discuss in Section 2.2.1) and configuration of liquid and solid phases as printing material at room temperature.[48] The DIW head consists of a dispenser with a nozzle at the exit. 3D parts are printed by moving the robotic arm to promptly print the computer-aided design (CAD) model in a layer form. Once the printing is completed, the next step is de-binding and sintering treatment to remove the binder content and to obtain maximum densification.[37,49,50]

The characteristics of the slurry are very important and vital for the extrusion printing. The feedstock is developed by combining fine solid powder particles (10–50 μm) with the binder material normally dispersed in deionized water or organic solvents in the presence of a range of additives,

including surfactants, dispersants and binders.[51,52] Blending and mixing of powders are usually carried out using tumbler mixers.[53] Furthermore, the viscosity is low enough to be extruded through the nozzle at comparatively low pressure. Meanwhile, the slurry must have sufficient yield strength and stiffness (storage modulus) to hold the shape. This is normally achieved by making the paste of binder/additives and ceramic powder with a volume fraction of the solid content higher than 50% to achieve maximum densification and to reduce dimensional inaccuracy in the final part. Shear-thinning behaviour is desired as it permits the slurry to be extruded through comparatively smaller diameter nozzles at relatively low pressure.[37] The special usage of solid slurries with essential viscoelastic behaviour permits the production of parts that can retain their initial shape irrespective of the force caused by the freshly deposited layers on top of them.[52] The beauty of DIW is its opportunity to fabricate structures with different configurations with complex parts and interconnecting cavities, to composite materials, solid monolithic components, and filaments with various cross-sectional forms.[54,55]

As previously discussed, the solid loading in DIW is normally greater than 50% in term of volume fraction to achieve maximum densification and to reduce dimensional inaccuracy in the final part, and typical ceramic slurries possess an average particle size from 1 to 100 μm.[52] Therefore, it requires a relatively larger nozzle size of 100–1000 μm than the inkjet printing system (~100 μm). According to Shahzad *et al.* the optimum diameter of the nozzle is generally 400–800 μm to avoid clogging of the slurry.[52] During the preparation of the slurry, an uniform dispersion of micro/nanoparticles has an important impact on the quality and morphology accuracy of the printed parts. Generally, the key criteria for achieving excellent printability *via* extrusion printing are the pseudoplastic behaviour of the slurry, its setting speed after dispensing, and uniform dispersion of the particles. One of the primary issues with DIW is ensuring a high-density printing without clogging the nozzle. This is generally solved through the promotion of a homogenous dispersion of the particles in the slurry and the use of a narrow particle range. To obtain narrow particle size distribution, a vibratory sieve is used to help removing large agglomerates. To fabricate high-resolution microscale prints, the particles sizes in the slurry must be an order of magnitude smaller than the final part resolution.

There are three main types of inks utilized in the robocasting of ceramic-based items:

(I) Gels and hydrogels, which generally are composed of an organic polymer that has been polymerized to create a macro polymeric 3D network swollen in water and enriched with solid particles. The downside of solid gel-based inks is the post-processing multistep required, including a well temperature control and laborious routes to obtain the desired 3D item.

(II) Organogels, a class of gels named as semi-solid systems with an organic phase immobilized by a 3D network formed by particles; and.

(III) Colloidal inks, which are stable suspensions of highly concentrated solid particles (60–80 wt%) in aqueous media (or by using other low-viscosity solvent), with a small quantity of organic compounds ≤1 wt% as surfactants, dispersants or polymers.[56] These inks need a significant amount of time to prepare them, involving the powder milling and stabilization of the colloidal powder required to achieve the desired rheology for having ink printability.[57–59] Obtaining the optimal rheological range for printing monoliths structures has been a challenge because general rheological printability conditions for ceramic materials have not yet been devised.

The formulation of these ceramic-based inks significantly affects the printability and mechanical strength of the structures. Hence, it is paramount to understand the characteristics of the ink because they are stabilised and interacted *via* different mechanisms, namely electrostatic, steric and electrosteric mechanisms (Fig. 2). Further discussion about the ink characteristics and optimisation can be found in the recent publication by Lamnini *et al.*[60]

2.2 Ink properties

Various factors, including the viscosity and density of the slurry, diameter and shape of the nozzle, printing speed, sintering method, and drying technique can significantly affect the final part properties and surface finish.[52] Among them, ink properties play the vital role in the printing process and finished product.

2.2.1 Physical change

2.2.1.1 The rheological behaviour of the slurry. The rheological behaviour of the slurry is the most critical attribute for printing 3D parts successfully, which means the desirable shape is retained as well as supporting the subsequent layers from collapsing under its weight (also known as slumping) without external assistance. The necessary rheological properties can be obtained through the appropriate choice of a binder-solid ratio. The flow behaviour of these slurries can be estimated by the model developed by Herschel–Bulkley. This model is based on ideal non-Newtonian fluids, which do not flow beneath

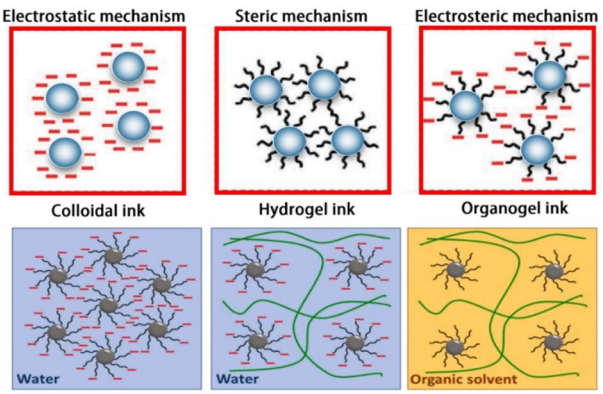

Fig. 2 Schematic diagram illustrating the three main mechanisms for particle stabilisation: steric and electrostatic interactions are represented with black lines and negative red charges respectively. Colloidal inks involve an electro-steric stabilization mechanism, which gives rise to polyelectrolyte complexes. The green lines represent the polymer chains within gel-embedded inks (reprinted with permission from ref. 60).

a particular stress (the yield stress). When the stress is increased to a certain level, they obtain shear-thinning behaviour where their viscosity declines significantly as the shear rate rises. Mathematically, it can be explained by the Herschel–Bulkley equation.

$$\tau = \tau_y + K\dot{\gamma}n \quad (1)$$

where τ is the shear stress being applied, τ_y is the yield stress, γ is the shear rate, n is the shear-thinning exponent and K is the viscosity parameter.

For DIW, a low value of n is advantageous so that the pressure of extrusion is fairly low and to encourage mixing. A low value of K is also necessary for similar purposes, whereas a high value of τ_y is required to avoid failure of the final part after the 3D printing process. Unfortunately, most of the above factors are firmly reliant on one another. So, controlling any of these parameters in isolation is a major challenge. Finding appropriate values of these parameters for robocasting is difficult because no such universal requirements exist. They entirely depend upon the shape and scale of the printed part, the diameter and shape of the nozzle, and the slurry density.[52,61] Hence, multi-physics simulation could provide a theoretical and optimization guidance in this regard (further discussed in Section 2.3).

2.2.2 Sol–gel precursors

2.2.2.1 Precursor sol–gel inks. Precursor sol–gel inks can be incorporated into the printing solution and post-treated to obtained crystalline ceramics. In this approach, the printed ink is based on sol–gel chemistry and uses an organometallic precursor in the form of a stable sol. The ink dries to form a xerogel layer that is further processed into oxide layers, usually by calcination. For precursor (sol–gel) inks, sol–gel chemistry parameters, such as precursor concentrations, type (*e.g.*, organometallic, such as titanium isopropoxide), and solvent must be considered. These parameters, and the gelation period, allow the viscosity of sol–gel inks to be tuned. Sol–gel chemistry also allows tuning of the final microstructure (*e.g.*, crystal phase or porosity). It should be noted that these systems differ from the inkjet printed sol-gels, which contain the preformed semiconductor nanoparticles.[45,62]

2.3 Multi-scale multi-physics simulation

Multi-scale and multi-physics simulations are normally conducted using Computational Fluid Dynamics (CFD). CFD is a powerful tool to understand physical flow behaviour, such as pressure patterns, slurry velocity distribution and slurry viscosity changes in the extrusion nozzle or syringe. Simulation studies have been previously used to predict the cross-sectional morphology formed by the successive deposition of parallel strands in material extrusion.[63] The simulation results provide a theoretical flow model that can be used to optimize for the apparatus design and operation. However, reported work did not consider the polymer chain folding during extrusion, but rather assumed the property uniform distribution in the extruded strand as well as the variation of mechanical properties, such as Young's moduli during extrusion (*e.g.*, solidification process during fabrication). Thus, the multi-scale multi-physics modelling of ink for DIW are required to incorporate and simulate all the fundamental processes, including flow, heat transfer, viscoelastic properties, solidification and crystallization that occur across various length of scales.[64]

2.3.1 Flow modelling. Flow modelling is normally related to the extruder design. DIW can be performed by three types of extruders:[65]

(I) The die is driven by the ram with the constant velocity as shown in Fig. 3a.

(II) The die is driven by the high constant pressure gas *e.g.*, N_2 as shown in Fig. 3b.

(III) The gel, paste or slurry is deposited by a screw extruder as shown in Fig. 3c.

Currently, most of CFD modelling focused on the extruders with constant ram velocity or constant pressure as illustrated in Fig. 3a and b, respectively.

The gel for direct writing is a typical non-Newtonian fluid. Due to the relationship between shear rate (γ) and shear stress (τ), as outlined in eqn (1), printing fluids are either Newtonian or non-Newtonian fluids. The shear rate is the change of velocity along the direction of material or flow deformation. The shear stress is the applied parallel or tangential stress to cause the material or flow deformation. The Newtonian fluid has a linear relationship of shear stress to shear rate with a constant viscosity. The non-Newtonian fluid has a nonlinear relationship between shear rate and shear stress, including shear thinning pseudoplastic fluid, shear thickening dilatant fluid, Bingham plastic fluid or Bingham pseudoplastic fluid.

Generally, CFD is employed for modelling Newtonian fluids, such as air and water using the Navier–Stokes's equations. For simulation of non-Newtonian fluids, the viscosity in the momentum equation for generalized Newtonian fluids is substituted by the non-Newtonian fluid model. Two scenarios can be considered for CFD simulation of DIW:

(I) The focus of modelling is on the ink flows in the extrusion nozzle or syringe, then a single fluid is applied for simplifying the mathematic problems without losing the accuracy.

(II) If ink deposition process and deposited strand morphology are focused on, the two fluids including gel and atmospheric air are applied for modelling.

To obtain clear interface between two fluids, gel and air, generally the volume of fluid method (VOF) is employed. The

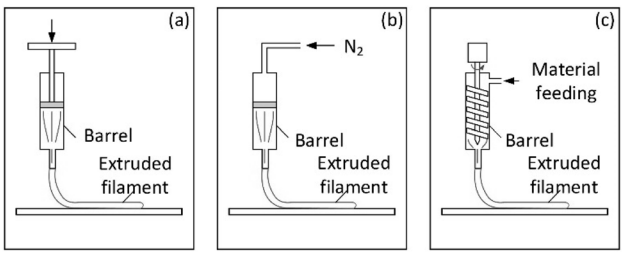

Fig. 3 Types of direct-writing extruders: (a) constant ram velocity; (b) constant pressure; (c) screw extrusion (adapted with permission from ref. 65).

general computational domains are shown in Fig. 4, including the extrusion barrel, extrusion nozzle and the operation chamber. The substrate is set as the moving wall with a velocity of v. The setting of the inlet boundary is based on the extrusion driven by the ram with constant velocity or by a constant high-pressure gas.

The extrusion governing equations are listed below.

Continuity equation:

$$\frac{\partial \rho}{\partial t} + \nabla \cdot \rho u = 0 \tag{2}$$

Momentum equation:

$$\rho\left(\frac{\partial u}{\partial t} + u \cdot \nabla u\right) = -\nabla p + \rho g + \nabla \cdot \left[\mu\left(\nabla u + \nabla^{\mathrm{T}} u\right)\right] + T_{\mathrm{A}} + S_{\sigma} \tag{3}$$

Volume fraction equation:

$$\frac{\partial \phi}{\partial t} + u \cdot \nabla \phi = 0 \tag{4}$$

where ρ is the fluid density; t is the time; u is the velocity; p is the pressure; g is the gravity; μ is the dynamic viscosity; S_{σ} is the surface tension; T_{A} is the viscoelastic stress due to the orientation of the polymer; φ is the phase volume fraction. S_{σ}, T_{A} can be ignored for small surface tension and viscoelastic stress.

For non-Newtonian fluids, the viscosity, μ, in the momentum equation is

$$\mu = f(\dot{\gamma}) \tag{5}$$

where $\dot{\gamma}$ is the shear rate.

In the flow, the shear rate can be worked out by the following equations.

$$\dot{\gamma} = \sqrt{2tr(D)^2} = \left(2\sum_i \sum_j D_{ij} D_{ji}\right)^{\frac{1}{2}} \tag{6}$$

$$\dot{\gamma} = \sqrt{\left|\dot{\gamma}_{xx}\right|^2 + \left|\dot{\gamma}_{yy}\right|^2 + \left|\dot{\gamma}_{xy}\right|^2 + \left|\dot{\gamma}_{xz}\right|^2 + \left|\dot{\gamma}_{yz}\right|^2} \tag{7}$$

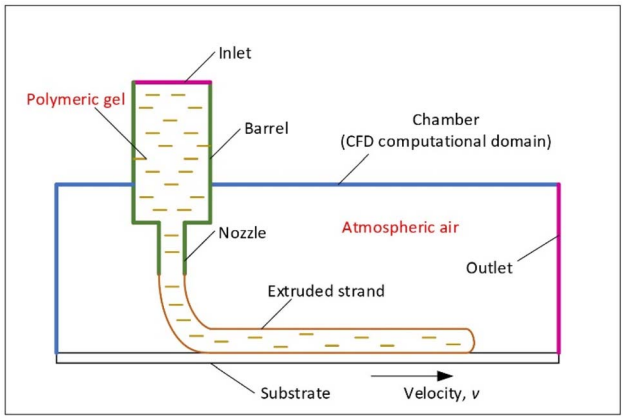

Fig. 4 Schematic diagram of direct-writing process and CFD computational domain.

where $D = \frac{1}{2}(\nabla u + \nabla^{\mathrm{T}} u)$ or $\dot{\gamma} = (\nabla u + \nabla^{\mathrm{T}} u)$.

There are two common methods to resolve these CFD governing equations, namely the finite volume method (FVM) and finite element method (FEM). Although FEM and FVM share some similarities, they have some differences in the ease of implementation. FVM is easier to implement that FEM according to the opinion of the majority of engineers. The FEM is a great method for Multiphysics analysis and complex geometries, however, the most significant advantage of FVM is that it needs to do flux evaluation for the cell boundaries. This makes FVM an excellent choice for solving non-linear conservative laws issues. The software developed based on these methods is divided into two categories: ANSYS FLUENT and open source OpenFOAM are based on FVM; whereas ANSYS POLYFLOW, FLOW-3D and COMSOL Multiphysics® are based on FEM.

Studies demonstrated that the cross-sectional morphology of the strand is well predicted by CFD modelling as shown in Fig. 5a. The cross-sectional morphology of the layered strands (Fig. 5b), the porosity of the deposited structure (Fig. 5c) and the strand overlapping (Fig. 5d) can be well simulated using CFD with the non-Newtonian fluid model.

The non-Newtonian fluid models simulated with CFD for DIW are further discussed below.

2.3.1.1 Pseudo-Newtonian model. When the non-Newtonian fluid flow is in the creep region, which is below its onset shear rate, the viscosity could be assumed to be constant as the Newtonian flow, so the pseudo-Newtonian model can be described as:

$$\mu = \frac{\tau}{\dot{\gamma}} = \text{constant} \tag{8}$$

where τ is the shear stress.

For instance, Serdeczny *et al.* numerically and experimentally investigated the polylactic acid (PLA) strand shape during

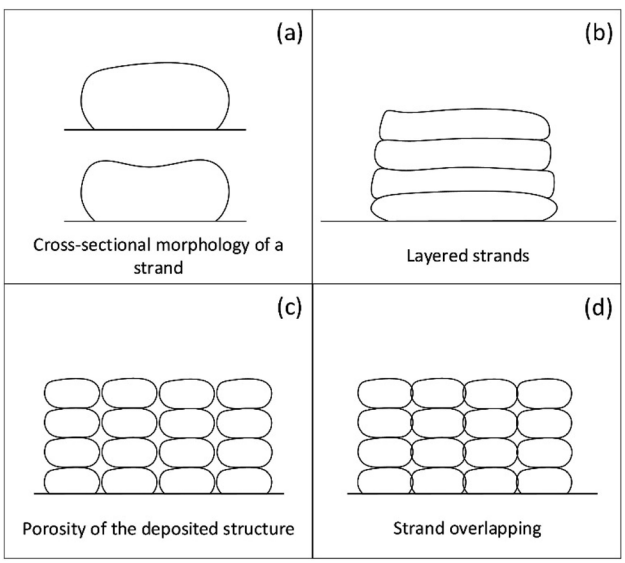

Fig. 5 CFD predicted the (a) cross-sectional morphology, (b) layered strands, (c) porosity and (d) overlapping of strands.

the extrusion process.[66] The PLA was extruded at 200 °C and deposited on a planar substrate at room temperature. The extrusion was treated to be in the creeping flow region. Since the viscosity was 1000 Pa s, the inertial effect was ignored. The simulation based on ANSYS FLUENT demonstrated that the predicted cross-sectional shape was in good agreement with the experimental measurements, showing the capability to predict the strand morphology for different extrusion conditions. Using the similar simulation approaches, the research group further investigating the relationship of the gap distance between the extrusion nozzle and the substrate, and the velocity ratio of the substrate to the average velocity of the flow inside the nozzle to the strand morphology.[67] They concluded that the printing force applied by the extruded material on the substrate had a negative linear relationship with the velocity ratio at a constant printing distance. In addition, the simulation showed that by decreasing the layer thickness and the strand-to-strand distance led to a smaller pores and larger inter- and intra-layer bond line densities.[66] Meanwhile, the surface roughness of the vertical and horizontal walls was improved with the decreasing of the layer thickness, in contrast, decreasing the strand-to-strand distance reduced the roughness of the horizontal surfaces. The quantitative predictions of the porosity, the bond line densities and the surface roughness opened the possibility of performing numerical optimizations of the process parameters. Furthermore, Narei *et al.* used ANSYS FLUENT to simulate the core–shell polymer strand in the extrusion process.[68] The viscosity for the molten shell and core polymer were fixed at 1000 and 1500 Pa s, respectively. The cross-sectional morphology of the strand was then studied under different printing speeds to find out the highest volume fraction of the core through changing the printing parameters. However, this pseudo-Newtonian model is only suitable for very low shear rate, such as flowing in the creeping region. For higher shear rate, other models, such as the power law must be applied.

2.3.1.2 Herschel–Bulkley (power law) model. For most printing processes, the shear thinning fluid can be described by the power-law equation. The shear stress is linear to n times of shear rate. For Bingham pseudo plastic fluid, the viscosity can be presented by Herschel–Bulley (power law) model as eqn (8).

$$\mu = \frac{\tau_0}{\dot{\gamma}} + k\dot{\gamma}^{n-1} \tag{9}$$

where τ_0 is the Bingham interception; k is the coefficient; n is the index.

Recently, Liu *et al.* simulated a single pseudoplastic fluid of wheat gluten and potato granules extrusion process by ANSYS POLYFLOW using the power-law model.[69] The pressure and viscosity distributions in the extrusion barrel were studied under different k and n values, which determines the flow field distribution. The validated model exhibited improved printing characteristic when the k value was between 1000 and 1800 Pa s^n and n value between 0.15 and 0.3. Last year, Song *et al.* used ANSYS FLUENT to model the extrusion of the jammed gelatin microgel as the Bingham pseudoplastic fluid. The constitutive behaviour of the microgel composite ink was captured for the first time after fit with Herschel–Bulkley model.[70] It was found that the cross-sectional shape turned into flat rectangular under a small normalized gap distance (less than 0.6 mm). Furthermore, the achievable maximum length (without collapse) of the jammed gelatin microgel-based composite ink, deposited both between two supporting substrates and over a supporting substrate, were evaluated and visualized. In addition, the self-supported filament printability was also evaluated using the same simulation method. Behdani *et al.*, who used OpenFOAM with the power-law model, investigated the cross-sectional morphology of the extruded PLA strand, which is sensitive to the viscosity, and the gas size between deposition nozzle and the planar substrate.[71] Papon *et al.* modelled the polymer fused filament fabrication through different nozzle geometries, such as circular, square and star shape, by the ANSYS FLUENT VOF method.[72] The flow was assumed laminar, non-isothermal and non-Newtonian with the power-law model fitted. The results showed that the melting polymer spreading characteristic was affected by the nozzle geometry.

With the limitation of very slow shear rate and very high shear rate at which the flow has a nearly linear relationship between shear stress and shear rate, the Herschel–Bulley (power law) model is only suitable for the intermediate shear rate ($0 < \tau < \infty$).

2.3.1.3 Cross model. In order to overcome the limitations of the power-law model, which fails to predict the Newtonian plateau at the viscosity under the very low and very high shear rates, the Cross model was introduced by M. M. Cross, in 1979 (ref. 73) as:

$$\mu = \mu_\infty + \frac{\mu_0 - \mu_\infty}{1 + (\lambda\dot{\gamma})^n} \tag{10}$$

The Cross model is an empirical equation that is used to fit non-Newtonian data. More specifically, this model "describes pseudoplastic flow with asymptotic viscosities at zero (μ_0) and infinite (μ_∞) shear rates, and no yield stress".[74] The Cross model can describe many types of fluids, including dispersions, polymer melts, and polymeric solutions. Using this method, Gosset *et al.* employed OpenFOAM VOF models to simulate melting poly-lactic acid (PLA) extrusion process at the temperature of 215 °C.[75] Through rheological experiments, the viscosity of melting PLA is better fitted with the Cross model compared to the power law model. The estimated extruded strand height and strand cross-sectional shape matched very well with the experimental measurement. In addition, Nikfarjam *et al.* introduced the cross model for non-Newtonian fluids into CFD simulation and developed Level-set-STAGgered (LS-STAG) cut-cell method, which showed its versatility even for the Xanthan flows in a 2 : 1 axisymmetric sudden expansion.[76] Antonietti *et al.* undertook the mathematical modelling of the polymer extrusion of hollow and non-hollow yarns by ANSYS POLYFLOW.[77] The flow was found to be non-Newtonian, incompressible and isothermal under these conditions. The cross rheological law was employed as constitutive model for the viscosity. The Cross model is popularly used for CFD simulations because it covers from very low shear rate to very high shear rate. However, since it is an empirical equation, the model may or may not be appropriate

for various applications. Hence, the Bird–Carreau model was introduced in 1987.[78]

2.3.1.4 Bird–Carreau model. The Bird–Carreu model has more parameters than the Cross model and is also a more generalized form of the power law fluid model. For cases where there are significant variations from the Power Law model, such as at very low and very high shear rate, it becomes essential to incorporate the values of viscosity at zero shear (μ_0) and at infinite shear (μ_∞) into the formulations (eqn (11)).[79]

$$\mu = \mu_\infty + \frac{\mu_0 - \mu_\infty}{\left(1 + (\lambda\dot{\gamma})^2\right)^{\frac{(1-n)}{2}}} \quad (11)$$

where μ_0 is the zero-shear viscosity; μ_∞ is the infinite shear viscosity; λ is the relaxation time.

To provide industrial insight on the printability of 3D printed materials, Guo *et al.* employed Bird–Carreau model for single fluid and studied the grain gel extrusion process within the syringe.[80] The simulations were performed using ANSYS POLYFLOW and clearly illustrated the transport behaviour, giving a more realistic understanding of the slurry flow during extrusion. Based on the simulation results, the piston pressure can be a criterion to evaluate the printing performance of different grain gels. However, Guo *et al.* suggested that the use of structural mechanics simulation would be helpful to evaluate the mechanical properties and structural stability of the printing materials. Ni *et al.* investigated the printing of flame retardant plastics, such as acrylonitrile–butadiene–styrene (ABS) and ammonium polyphosphate (APP), by applying a numerical approach using finite element (FEM)-based software, COMSOL Multiphysics®, aiming to overcome nozzle clogging and establish optimal three-dimensional (3D)-printing parameters.[81] The fully melted ABS or APP was fitted to the Bird–Carreau viscosity model showing the temperature distribution, melting evaluation, pressure and velocity distribution in the nozzle for the 3D printed flame retardants. Yilmaz *et al.* proposed that the wall shear rate and shear stress, flow uniformity at the die exit and pressure drop through the dire were the critical factors for designing plastic extrusion dies.[82] By employing ANSYS POLYFLOW and the Bird–Carreau model as the viscosity model for the polymer melt, the 3D CFD analyses provided a comprehensive understanding of the polypropylene (PP) melt flow through the conical spiral mandrel die.

Achieving a balanced flow is one of the major challenges during the profile design of extrusion dies.[83] For this purpose, numerical modeling codes may be a very useful aid. Gonçalves *et al.* developed CFD code to model the flow of polymer melt to deal with unstructured meshes.[84] The Bird–Carreau constitutive equation was employed to model the shear viscosity dependent on shear rate. The self-compiled code was verified by the problem of Lid-driven cavity. The developed code had been a valuable tool to aid the design of complex profile extrusion die with improved the flow distribution. Although the Bird–Carreau model has not been employed to simulate the extrusion process of DIW, it can be used for the wide range of shear rate. Therefore, the Bird–Carreau model can be employed in the CFD simulation of direct writing.

2.3.2 Heat transfer. Heat transfer plays an important role in extrusion-based 3D printing methods as the filament must be melted to flow through the nozzle and heat transfer process takes place to allow solidification of the printed object. Additionally, the inter-road adhesion or welding is controlled by the thermal profile of the nozzle through to deposition. One-, two- and three-dimensional heat transfer models have been used to model heat transfer processes. Time-dependent 1D heat transfer models including conduction and natural convection have been used to study the strength of inter-road bonds.[85] Although 2D modelling approach can potentially provide more insight than 1D modelling, it is not sufficient to accurately predict temperature gradient within the deposition boundary.[86,87] However, 3D heat transfer modelling using high performance computing facilities has made it possible to simulate the thermal profile within the nozzle head or rapid cooling in deposition process as reported by Wang *et al.*[88]

There is no doubt that modelling and simulation have significant contribution in characterizing and optimizing the whole process of 3D printing. However, it is crucial to validate numerical models *via* comparison to experimental results. Several studies have shown good agreement between modelling and experiment results. For instance, Luo *et al.* recently developed a heat transfer model, which provided an upper limit of the polymer feed rates.[89] They also performed experiments on a modified extruder setup to obtain experimental results and validate their model. The modelling and experimental results matched well especially for a nozzle wall temperature range of 210–260 °C. Meanwhile, Coasey *et al.* used interlaminar fracture toughness measurements to validate a non-isothermal welding model, which predicted the healing over time by considering the effect of processing parameters and rheological properties.[90] The model and the experimental results provided a good fundamental knowledge for future printer development.

A post-extrusion heating model was recently developed by Edwards and Mackay to minimize the formation of surface roughness called shark-skin defects for both amorphous and semi-crystalline polymers during material extrusion.[91] Shark-skin defects can reduce the effectiveness of binding the polymer to the underlying substrate. They investigated one potential solution for this problem, which is reheating the polymer after it exits the hot end extrusion nozzle. This process allowed the polymer to relax more before deposition. They also performed experiments and observed that the shark-skin defects are reduced once the polymer has reached a certain temperature.

The heat transfer in the polymer melt is significantly affected by the rheological properties which control the flow characteristics.[92] For instant, heat transfer can affect the differential pressure across the nozzle and reduce the printing speed as it was shown by a rheological behaviour modelling performed by Phan *et al.*[93] It is essential to employ a multiphysics modelling approach to account for coupling effects of different effective physics in the 3D printing process.

3. Printing of functional materials by DIW

Global energy and environmental crises are among the most pressing challenges facing humankind. To overcome these challenges, recent years have seen an upsurge of interest in the development and production of renewable chemical fuels as alternatives to the non-renewable and high-polluting fossil fuels. Photocatalysis, photoelectrocatalysis, and electrocatalysis provide promising avenues for sustainable energy conversion.[94] Various effort and design have been devoted for DIW extrusion-based printing to produce fine and complex 3D architectures as reviewed by Lewis.[95] Recently, Fu *et al.* summarised the research efforts on the use of DIW and development of graphene oxide (GO) based inks to fabricated structures for energy storage, electronic circuits and thermal energy applications.[39] Furthermore, Zhakeyev *et al.* highlighted the DIW-based studies on the development of 3D microstructured materials for different energy storage and conversion applications.[17]

3.1 Photocatalysts

Photocatalysis, which is the most typical wireless systems and is the easiest systems among different configurations (*i.e.*, photocatalysis (PC), photoelectrocatalysis (PEC) and electrocatalysis (EC), offers new and timely opportunities for renewable energy generation, environmental remediation, and 'green' chemical synthesis.

While the usage of photocatalysts has been growing during the last decades as summarized in Table 1, there are still relatively few cases reported of printed materials being used in this area of interest *via* robocasting,[12,96–99] because the integration of AM and catalysis is still relatively new. The amount of published work only started to emerge in 2015.[100] To date, different photocatalytic applications, such as photodegradation of pollutants in liquid or gas system, and chemical conversion to synthesize value-added molecules, like H_2 or NH_3, have been developed. This new trend of technological tailormade developments allowed users to obtain more specific materials, simplifying their design and application in complex reactor systems, and increasing their efficiency or equalling the photocatalytic activities of their powdered counterpart.[101]

A good photocatalytic material should involve a good charge separation, a fast charge transfer, absorption in the visible light spectrum of the UV-Vis range, high stability, low cost, and nontoxicity.[94] Hence, the development of photocatalytic 3D printed materials should take into account all these properties. Furthermore, it is important to highlight that 3D printed photocatalytic designs should facilitate their use compared with conventional materials, including powdered materials, thin films, or coatings, and could be applied in pilot and/or industrial scales.

TiO_2 powder-based systems have been extensively reported for PC, PEC and EC applications. However, the powder-based systems limit the recyclability and reusability of TiO_2 materials. 3D-printed hierarchical porous TiO_2 structures featuring a printed macrosized grid or cellular structures, porous microstructures, and a specific structural strength have shown great potential in many applications, including water treatment and catalyst carriers. The main aim of this section is to summarize the new trends and approaches related to 3D printing of catalysts and their photocatalytic applications for dyes degradation, H_2 production, and air purification.

Compared to powder-based materials, thin films, or photocatalytic coating systems, the 3D-printed monolith structures are easy to reuse due to their high structural strength, which is critical for practical use. The design of the photocatalysts may take any shape once the necessary rheological properties of the inks have been achieved. However, the DIW technique is such a broad and virgin field for the development of photocatalyst 3D printed materials and is going to impose as an affordable tool to magnify the outstanding application in the very near future. The first monolithic structures created using 3D printers were solid support structures based on titanium using a direct manufacturing process called Robocasting. Duoss *et al.* created the first 3D printed TiO_2 microstructures using sol–gel precursor solutions containing chelated titanium alkoxide and polyvinylpyrrolidone (PVP) as the polymer additive.[102] Recently, a binder free design of TiO_2 ceramic pastes was reported by Bonilla-Cruz *et al.*[103] The study performed a systematic investigation on the rheological properties of TiO_2 paste was conducted by adjusting the volumetric ratios of water and glycol, demonstrating for the first time a straightforward, facile, and environmentally friendly technique to produce a printable (viscosity range: $1 \times 10^5 \leq \eta \leq 9.9 \times 10^5$ Pa s) and self-supporting monolith by DIW. The study emphasized that a shear-thinning behavior and a gel-point ($G' = G''$) $> 1 \times 10^3$ Pa were crucial to obtain three dimensional and self-supported complex ceramic structures with excellent shape-retention. The binder-free three-dimensional ceramic structures exhibited good mechanical stability after 400 °C drying process.

TiO_2 has been extensively used as a photocatalyst for the purification of water and air, and self-cleaning surfaces purposes. Furthermore, due to its high oxidation activity and super hydrophobicity, TiO_2 can be employed as an antibacterial agent. TiO_2 has a relatively high degree of reactivity and chemical stability when exposed to UV light (387 nm) with an energy greater than the band gap of the anatase crystalline phase, which is 3.3 eV.[104] Recent development using TiO_2 and other inorganic ceramic precursors for DIW for 3D printed monoliths and their photocatalyst performance are summarized in the Table 2.

3.1.1 TiO_2 monoliths. TiO_2 has been extensively used in various photocatalytic applications. To demonstrate and increase the potential of 3D printed monolithic titania, Elkoro *et al.* showcased that a combined robocasting and low temperature chemical sintering (150 °C) method was feasible to fabricate 3D TiO_2 monolith in the absence of a binder.[98] The TiO_2 monoliths showed strong photocatalytic activity during the breakdown of acetaldehyde to CO_2 and H_2O during an air purification procedure. The concentration of acetaldehyde eliminated varied according to its concentration in the gas phase. The yield for acetaldehyde at 5000 ppmv was 40–58%, whereas the yield for acetaldehyde at 70 000 ppmv was around

Table 2 Photocatalytic applications of 3D printed monoliths obtained by DIW

Material	Comments	Results/applications	Ref.
TiO_2	Mass: 0.5 g Figure: square lattice Concentration of reactants: liquid 10 mg L^{-1} and gas 63% of propane, 7% of isobutane, and 30% of *n*-butane on a molar basis Light source: liquid, 150 mW cm^{-2} (380–780 nm); gas, 1680 μW cm^{-2} (200–280 nm) Adsorption time: 30 min equilibrium in dark Degradation time: 4 h liquid; 15 h gas pH: 7.0	Liquid degradation of triclosan 99.5% Gas degradation of *n*-butane 95.3% Isobutane 93.7% Propane 52.9%	101
	Mass: 1.25 g Figure: monolith cylinder Concentration of reactant: 5000 ppmv with a flow rate of 20 mL min^{-1} Light source: 84 mW cm^{-2} Adsorption time: 8 h equilibrium Degradation time: 30 min pH: not specified	40–58%, acetaldehyde degradation	98
	Mass: 22 g Figure: square-lattice double-diagonal (13.5 × 13.5 cm) Concentration: 20 mg L^{-1} of acesulfame potassium Light source: solar simulator, 1500 W, Xe arc lamp, wavelength range 280–800 nm, 15 mW cm^{-2} Adsorption time: not evaluated Degradation time: 60 min pH: 7.3	Degradation of acesulfame potassium (99.99%)	105
	Mass: not specified Figure: cube grille (10 mm × 10 mm) Concentration of reactant: 30 mL min^{-1} of N_2 Lamp: 300 W Xe lamp, 100 mW cm^{-2} Equilibrium time: 1 h in dark Time reaction: 6 h pH: not specified	NH_3 production 7.4 nmol h^{-1}	99
Au/TiO_2 (Au 1.0 w%)	Mass: not specified Figure: circle mesh (24 cm^2) H_2 production: water/ethanol Concentration: 90/10 ratio Light source: UV LEDs (58 mW cm^{-2}) Reaction time: 12 h	H_2 production 0.24 mol min^{-1} g_{Au}^{-1}	12
α-Fe_2O_3	Mass catalyst: not specified Figure: woodpile structure (14 mm × 14 mm and 8 mm) Concentration: 2 mg L^{-1} of methylene blue Lamp: 50 W (280–450 nm) Adsorption time: not specified Degradation time: 60 min pH: not specified	Degrade 60% of methylene blue	96
g-C_3N_4/PEGDA	Mass catalyst: not specified Figure: patterned mesh 3D air filter spacing of 0.8 mm and size of 2 × 2 cm^2 Concentration of reactant: 550 ppb NO (humidity RH 75%) 3.0 L min^{-1} Lamp: LED lamps (420 nm, 20 mW cm^{-2}) Adsorption time: not specified Degradation time: 60 min pH: not specified	NO removal rate of 52.6% could be used continuously for more than 80 h	97
Fe_2O_3/GO	Mass: 7.2 mg Figure: Square length (7.5 mm and a thickness of 1.2 mm for 8 layers) Concentration of reactant: 0.02 mmol L^{-1} of RhB Lamp: 100 mW cm^{-2} solar simulator Adsorption time: 4 h Degradation time: 120 min pH: 5.2	97.8% of RhB after 120 min	106

8%. In the following year, Elkoro *et al.* used the same binder-free colloidal ink method to fabricate an Au/TiO_2 monolith for hydrogen photoproduction.[12] The monoliths impregnated with Au after 3D printing (*i.e.*, post-impregnation) exhibited much higher efficiency compared to non- and pre-impregnated monoliths on the rates of hydrogen photoproduction. The best photoactivity was found at 0.24 mol min^{-1} $g_{Au}{}^{-1}$.

The ink development using environmental benign solvent, such as water, has been also reported. For instance, Mendez-Arriaga *et al.* developed the solid square-lattice double-diagonal structures (SLDD) using only water as a solvent to prepare the ink and evaluate the photocatalytic activity through the degradation of acesulfame potassium (ACE). The SLDD manufactured TiO_2 showed 99% and 79% removal of 20 mg L^{-1} of ACE in solution within 60 min of UV-vis irradiation by using 0.5 and 22 g L^{-1} of TiO_2 in slurry and SLDD form, respectively.[105] Meanwhile, Ávila *et al.* fabricated the three-dimensional structures from TiO_2 nanoparticles using a mixture of volumetric ratios of water and glycol 50 : 50, and subsequently dried at 400 °C for 6 h.[101] The binder-free monoliths were evaluated for the photodegradation of triclosan in liquid phase and light-weight hydrocarbons in gas phase. The 3D printed square-lattice monoliths shown 99.5% of triclosan photodegradation and >90% of total organic carbon mineralization after 240 min under UV-Vis LED light irradiation. Also, it is noteworthy to highlight that this material was used in 12 consecutive cycles without significant deterioration on the photocatalytic activity. On the other hand, in gas phase this material presents an efficiency of photodegradation around 95.3, 93.7 and 52.9% for *n*-butane, iso-butane and propane; respectively, demonstrating the versatility of these monolithic structures for liquid and gas phases photodegradation of emergent pollutants.

3.1.2 Others inorganic monoliths. Other inorganic monoliths, especially α-Fe_2O_3, have been fabricated using robocasting approach to create 3D structures. For instance, Li *et al.* produced 3D α-Fe_2O_3 woodpile structures by using the aqueous-based solid ink using DIW method.[96] Additionally, cellulose was added to the suspension to improve the performance of the final ink. Once printed, the green body structures made of the raw α-Fe_2O_3 structure were dried for 48 h at ambient temperature and then sintered for 2 h at 800 °C in an air environment at a heating rate of 3 °C min^{-1}. The α-Fe_2O_3 monolith showed a good performance in accelerating the degradation of 60% of methylene blue (MB) solution in 1 h. Meanwhile, Wang *et al.* used an innovative microgel template-assisted solvothermal method to fabricate a micro-reactor that consisted of hollow α-Fe_2O_3 microspheres and graphene.[106] First, poly(*N*-isopropyl acrylamide-acrylic acid) P(NIPAM-AA) microgel spheres were synthesized by free radical polymerization, using *N*,*N*′-methylenebisacrylmide (BIS) as a cross-linker, and sodium dodecyl sulfate (SDS) as a surfactant. Next, $FeCl_3 \cdot 6H_2O$ (90 mg) was added to the microgel spheres to synthesize hollow α-Fe_2O_3 microspheres. The developed material had a photocatalytic degradation efficiency of rhodamine B of 97.8% when exposed to simulated sunlight for 120 min.

Using 3D DIW printing technique, Xu *et al.* created a polymeric air filter made of g-C_3N_4/poly-(ethylene glycol) double acrylate (PEGDA) nanocomposite for nitrogen oxides (NO_x) removal.[96] The photocatalyst g-C_3N_4 serves as starting material, while the PEGDA served as the role of both dispersant and matrix to form an optimal ink. The as-printed structure was dried using a simple freeze-drying method. The fabricated air filter demonstrated excellent photocatalytic performance (52.6% of NO_x removal) and long durability (up to 40 h).

Noticeably, compared to powder-based materials, thin films, or photocatalytic coating systems, the 3D-printed monolith structures are easy to reuse due to their high structural strength, which is critical for practical use. The design of the photocatalysts may take any shape once the necessary rheological properties of the inks have been achieved. However, the DIW technique is such a broad and virgin field for the development of photocatalyst 3D printed materials and is going to impose as an affordable tool to magnify the outstanding application in the very near future.

3.2 Photo(electro)catalysts

In recent years, TiO_2 has been demonstrated to be able to perform photocatalytic nitrogen fixation due to its high photocatalytic activity, excellent chemical stability, easy preparation into versatile morphologies, environmental friendliness, and low cost.[107,108] Li *et al.*, demonstrated that the 3D printed hierarchical porous TiO_2 structures could be used as an effective photoelectrode for N_2 reduction without electric bias.[109] The conversion efficiency of N_2 to NH_3 in the single photoelectrochemical cell was significantly enhanced when the 3D printed TiO_2 substrate was modified with surface oxygen vacancies and decorated with gold nanoparticles, which exhibited a surface plasmon resonance effect. Xu *et al.* then prepared 3D hierarchical porous TiO_2 structures (namely nanoparticles, micrometer-particles, and nano/microparticles inks in an aqueous solution of Pluronic F127, Fig. 6a) using powder-based inks for photoelectroreduction of N_2.[99] The use of powder-based inks offers good printing flexibility because the printing can be performed in an air environment without the need for an additional solidification treatment. The obtained porous TiO_2 scaffold structure (Fig. 6b) printed with nano/microparticles inks exhibited the highest N_2-to-NH_3 conversion efficiency (7.4 nmol h^{-1}); whereas the solid cube exhibits only 5.0 nmol h^{-1} of NH_3 production (Fig. 6c).

3.3 Electrocatalysts

Energy storage in the form of hydrogen (H_2) – a carbon free carrier with high energy density, has been proven to be a potential technique for intermittent energy storage. The development of active, durable, low-cost, earth-abundant electrocatalysts is vital to make this technology more viable and widespread.[110] Although the catalyst development for H_2 has been extensively conducted, the use of DIW technology to create 3D catalytic electrodes for electrochemical application in energy conversion is still at its infancy stage. A recent study demonstrated the use of DIW to fabricate a porous 3D printed graphene sheet/MoS_2 aerogel as the cathodic material for H_2 evolution reaction.[111] The 3D printed porous network, which

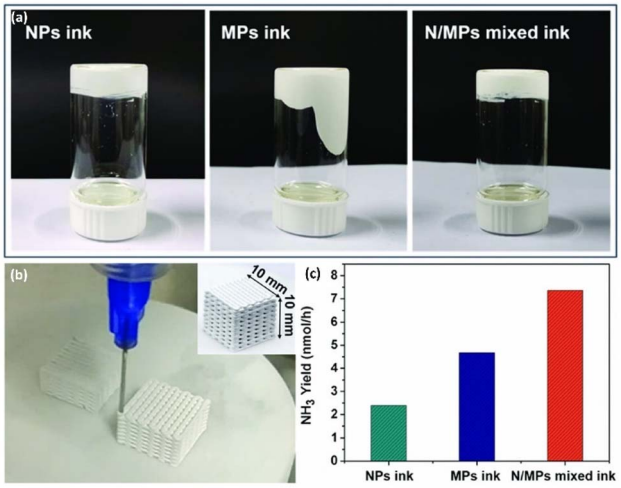

Fig. 6 (a) Optical images of the nanoparticles (NP ink), micrometer-particles (MP ink), and nano/microparticles inks (N/MP mixed ink; contains 20 wt% of NPs with respect to MPs) with a TiO_2 loading of 50 wt% in an upside-down vial). (b) Optical image of the 3D printing of the TiO_2 scaffold. The inset is an optical image of a representative TiO_2 cube scaffold with 20 layers and a side length of 10 mm. (c) NH_3 production over 6 h obtained from different TiO_2 scaffolds printed from different inks under light with an intensity of 100 mW cm^{-2} (AM1.5) (reproduced from ref. 99 with permission).

exhibited 1–2 nm of pore diameter, had shown to be a robust functionalised aerogel that provided multidimensional electron transport channels that improved the electronic conductivity; electrolyte dispersion that facilitated catalyst utilization.

Integration of 3D printing and dealloying in the process of making monolithic nanoporous metals has improved the performance of the catalytic processes for energy applications. Monolithic nano-porous metals provide large surface area and high electrical conductivity due to their unique solid/void structures. However, their performance can be improved significantly with an engineered hierarchical macroporous network structure, which results in increased mass transport. Zhu *et al.* combined direct ink writing with alloying and dealloying processes to create hierarchical nanoporous metal architectures composed of nanoparticle Au with engineered nonrandom macroarchitectures.[112] They managed to have both macro (10 to 1000 μm) and nano (30 to 500 nm) scales structures in the materials. Their printed nanoporous metals showed noticeable improvement mass transport and reaction rates for both liquids and gases. This has made the extrusion-based 3D printing DIW applicable to creating hierarchical nano-porous metal architectures.

Meanwhile, Ahn *et al.* utilised DIW to fabricate 3D graphene pyramids and then deposited Cu conductive layer and NiFe-LDH subsequently using electrochemical deposition method on the printed pyramid for electrochemical water splitting (Fig. 7a).[113] The obtained catalysts, which showed homogeneous coating of NiFe-LDH on the pyramids (Fig. 7b), exhibited a comparable electrocatalytic activity when compared to conventional NiFe-LDH samples reported in the literature and excellent durability without significant potential decay for 60 h. The structured photo(electro)- and electrolytic materials printed by DIW are summarised in Table 3.

The use of DIW to fabricate the electrocatalysts and photo(-electro)catalysts have not been extensively explored although

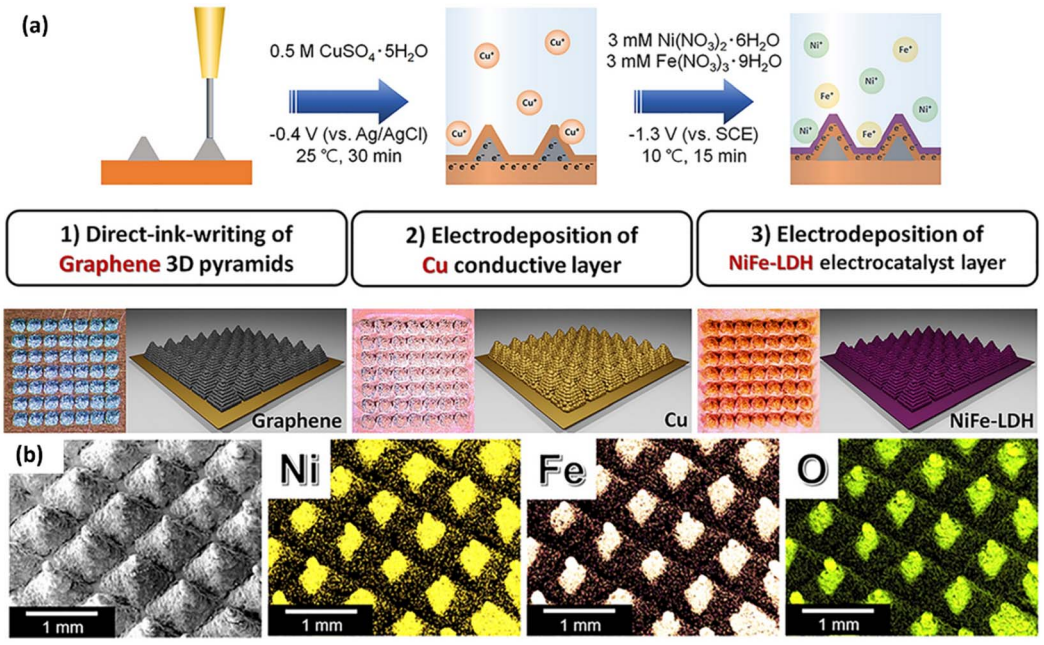

Fig. 7 (a) Schematic illustration of the fabrication of 3D-printed pyramid electrodes for OER in three successive steps. (1) Direct-ink-writing of graphene 3D pyramid array, electrodeposition of (2) Cu conductive layer and (3) NiFe-layered double hydroxide (LDH) electrocatalyst layers. (b) Energy dispersive spectrometry (EDS) mapping images of NiFe-LDH pyramid electrode: Ni (yellow), Fe (apricot), and O (green) (reproduced from ref. 113 with permission).

Table 3 Photo(electro)- and electrocatalysis applications of materials printed by DIW

Material	Fabricated structures	Applications	Ref.
Photo(electro)catalysis			
TiO_2	Hierarchical porous	N_2 photo(electro)reduction	109
	Porous scaffolds	N_2-to-NH_3 photoelectroreduction	99
Electrocatalysis			
Graphene sheet/MoS_2 aerogel	Porous aerogel	H_2 evolution reaction	111
Au	Nano-porous monolith	Selective oxidation of methanol	112
3D graphene deposited with Cu and NiFe-LDH	3D pyramid array	Electrochemical water splitting	113

many DIW-printed catalytic materials have been proposed and patterned for various applications, including thermochemical processes, chemical conversion and electricity production, as summarised previously.[100] As discussed in Section 2.1, there is a high interest of developing DIW for photo-, photo(electro)-, electrocatalytic materials and this is due to its rapid prototyping, concise design and cost effective. However, the printed materials often showed inferior performance than the pristine powdered materials. Hence, the development of new hybrid formulations, in which printable catalysts or precursors that can be transformed into catalysts in successive stages, will be the key to resolve this bottleneck, preserving their catalytic performance.[100]

4. Reactor design and fabrication

AM technology is also called rapid prototyping or freeform fabrication to 'print' 3D from 3D digital models instead of cutting materials from an initial bulk.[114,115] Due to its potential to offer reduced fabrication cost and time-efficient parts with complex 3D structure, AM has received significant attention to fabricate reactors for various energy conversion and environmental remediation applications.[99] Their general features and significance in designing a reactor for a specialised, well-defined application include:[116]

- Moderate capital and running costs, require low-cost components, a low cell potential difference (*i.e.*, particularly for electrochemical cells) and a low-pressure drop over the entire cell including the inlet and outlet flow manifolds for the reaction solution (*i.e.*, electrolyte for the case of an electrochemical cell); where possible, an undivided reactor that will simplify the engineering design and will lower the capital and running costs.
- Convenience and reliability, adequate design, installation, operation and maintenance and monitoring procedures.
- Appropriate engineering equipment for controlling and monitoring concentration, potential, current density (*i.e.*, particularly for electrochemical cell) and adequate mass transport regime to provide and remove reactants and products respectively, *via* flow distributions.
- Simplicity and versatility are perhaps the least quantified and most overlooked, yet the most important, factors for achieving an elegant and long-lasting design to attract users. Provision for the future by designing a modular configuration that can be scale-up by adding unit cells or by increasing the size of each unit.

Microchannel reactors provide for the catalyst component and fine control over reactant flow.[34] They have high surface to volume ratios, superior mass and heat transfer rates to conventional packed bed reactors, good laminar flow, small molecular diffusion distances, more homogeneous spatial illumination (*i.e.*, in the case of photocatalysis and photo(-electro)catalysis), and good reactant penetration throughout the catalyst bed.[117,118] A few 3D printing approaches have been used to fabricate microchannel reactors, as outlined by Friedmann *et al.*[44] Meanwhile, Yusuf *et al.* have reviewed the graphene-based materials in microfluidic photoreactors, which are potential efficient visible light photocatalysts. Zhakeyev *et al.* summarised the development of solar cells and photoreactors.[17] The development of DIW-printed reactor has also been reported since last decade. For example, Potdar *et al.* designed porous milli-scale reactors for optical measurements and chemical

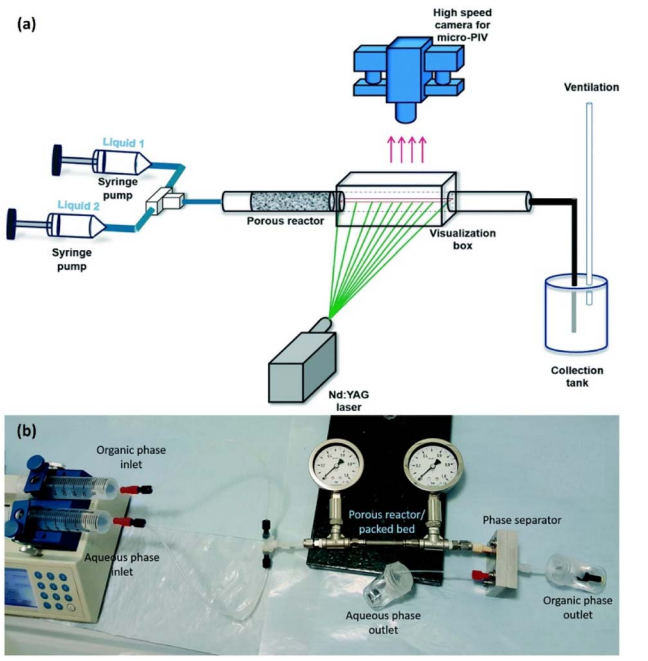

Fig. 8 (a) Schematic representative of experimental setup of optical measurements and (b) photograph of experimental setup of chemical mass transfer experiments (reprinted with permission from ref. 119).

system (Fig. 8). The porous reactor showed an enhanced mass transfer performance with an order of magnitude reduced energy dissipation compared to conventional milli-scale packed bed reactors.[119]

5. Perspective

A range of new DIW applications have emerged over recent years, and it is envisioned that 3D printing will continue to be utilized in manufacturing tandem to traditional fabrication approaches.[22] While 3D printing may offer an effective solution in the design of catalyst and rectors for performance testing, it is immensely beneficial for proof-of-concept and fundamental studies. Although such design may introduce further barriers to up-scaling and widespread adoption of the technology, the ability of DIW for rapid prototyping of the catalyst as well as micro-reactor provides a great research tool for industrial deployment especially in the fast emerging energy and environmental industries (Fig. 9). Once optimal designs are achieved, the technology be translated to processes, which are suitable for large-scale manufacturing. Typically, these processes require significant cost to set up (capital expense), but the operational expense of producing each unit is generally low. While today's additive fabrication technologies tend to have high operational expenses per unit, this is dropping and, depending upon the product, it is envisioned that manufacture will involve a combination of traditional and additive manufacturing technologies, while wholly printed structures will remain economically unviable for mass production in the short to medium term.[22]

In theory, DIW process can be introduced to most of the materials, as long as these materials can be extruded or sintered. The active component distribution can also be highly designed through modelling and customized using DIW. Different catalysts can be distributed in different regions of the catalyst structures to complete complex reactions. This greatly enriched the traditional catalytic materials. For example, during some exothermic reactions (*e.g.*, CO_2 hydrogenation to methanol), heat accumulation may happen in certain region of the catalyst bed, which will reduce the yield of the objective product (*e.g.*, methanol) in these reaction sites. Additionally, the 3D printing process achieves the preparation of fine structures with a relatively low cost. The structures can be customized and strictly controlled, and the complex manufacturing processes needed for conventional preparation methods are avoided. The prices of 3D printers and printing feedstocks are dropping rapidly in recent years. The cost of printed catalyst has the potential of being reduced to a reasonable range, which is crucial for industrial applications. At the same time, target structures can be carefully designed to fit the reaction system, such as monoliths, and an accurate rendering of the design can then be easily achieved. This makes the 3D printing process suitable for industrial use. Another potential use for DIW is in the preparation of microreactors. With 3D printing, the boundary between a catalyst, its support and reactor body are no longer very clear. The printed structure not only provides the catalyst component, but also controls the flow of the reactants. This may bring a significant enhancement to catalytic systems. Furthermore, the control of the microfluidic properties of the reactants helps to achieve good reaction performance with low cost. In addition, DIW, as a flexible approach, is also suitable for catalyst development. The printing process is applicable to small batch production and laboratory operations, which provides a great research tool for rapid prototyping, allowing to investigate and to optimize all kind of structures with a variety of porous materials. Accurate control of the structure and distribution of catalyst components is expected to bring a big improvement to the catalytic industry.

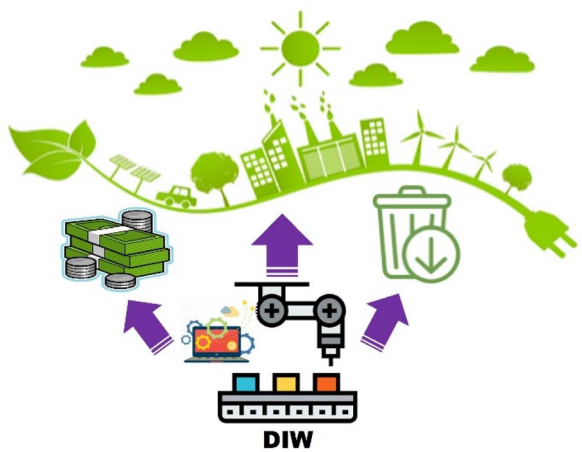

Fig. 9 Outlook of DIW.

6. Summary

With the depletion of fossil fuel resources and increasing environmental concerns, advanced catalysts are playing more important roles in many areas. The market for catalysts with novel structures will continue to grow in the future. As a bottom-up method, 3D printing fabrication provides new solutions for preparing catalysts with new multi-scales structures in a more economical and energy-efficient way.[34] As a new rapid fabrication method, DIW brings many new possibilities to the field of catalysis. Structural design, control of catalyst distribution, and the fabrication of monolithic reactors are becoming easier. However, further optimisation on the catalyst design and processing parameters are still needed to achieve required mechanical properties and even better catalytic performances for energy conversion and environmental remediation applications. Hence, insight on process simulation as well as artificial intelligent for DIW could probably aid the development of DIW with superior structure design and catalytic performance.

Conflicts of interest

There are no conflicts to declare.

Acknowledgements

The authors/we would like to acknowledge that this work was supported by the UKRI ISCF Industrial Challenge within the UK

Industrial Decarbonisation Research and Innovation Centre (IDRIC) award number: EP/V027050/1. Tania E. Lara-Ceniceros, José Bonilla-Cruz and Manuel Alejandro Ávila López would like to thank Centro de Investigación en Materiales Avanzados S.C. (CIMAV), for funding the Internal Project No. 23005 that supported this research. Manuel Alejandro Ávila López wants to thank CONACYT for the Postdoctoral scholarship, CVU 707526.

References

1 Summary for Policymakers of IPCC Special Report on Global Warming of 1.5°C approved by governments, https://www.ipcc.ch/2018/10/08/summary-for-policymakers-of-ipcc-special-report-on-global-warming-of-1-5c-approved-by-governments/#:~:text=Globalnethuman%2Dcausedemissions,removingCO2fromtheair.
2 AF2792-12a, *Standard Terminology for Additive Manufacturing Technologies (Withdrawn 2015)*, ASTM International, West Conshohocken, PA, 2012, DOI: DOI: 10.1520/F2792-12A.
3 S. A. M. Tofail, E. P. Koumoulos, A. Bandyopadhyay, S. Bose, L. O'Donoghue and C. Charitidis, *Mater. Today*, 2018, 22–37.
4 Q. Yan, J. Li, J. Zhang and Z. Cai, *Polymers*, 2018, **10**, 729.
5 A. Ambrosi and M. Pumera, *Chem. Soc. Rev.*, 2016, **45**, 2740–2755.
6 X. Tian, J. Jin, S. Yuan, C. K. Chua, S. B. Tor and K. Zhou, *Adv. Energy Mater.*, 2017, **7**, 1700127.
7 C. Zhu, T. Liu, F. Qian, W. Chen, S. Chandrasekaran, B. Yao, Y. Song, E. B. Duoss, J. D. Kuntz, C. M. Spadaccini, M. A. Worsley and Y. Li, *Nano Today*, 2017, **15**, 107–120.
8 F. Zhang, M. Wei, V. V. Viswanathan, B. Swart, Y. Shao, G. Wu and C. Zhou, *Nano Energy*, 2017, **40**, 418–431.
9 T. D. Ngo, A. Kashani, G. Imbalzano, K. T. Q. Nguyen and D. Hui, *Composites, Part B*, 2018, **143**, 172–196.
10 P. Chang, H. Mei, S. Zhou, K. G. Dassios and L. Cheng, *J. Mater. Chem. A*, 2019, **7**, 4230–4258.
11 Q. Zhang, J. Zhou, Z. Chen, C. Xu, W. Tang, G. Yang, C. Lai, Q. Xu, J. Yang and C. Peng, *Adv. Eng. Mater.*, 2021, **23**, 2100068.
12 A. Elkoro, L. Soler, J. Llorca and I. Casanova, *Appl. Mater. Today*, 2019, **16**, 265–272.
13 C.-Y. Lee, A. C. Taylor, S. Beirne and G. G. Wallace, *Adv. Energy Mater.*, 2017, **7**, 1701060.
14 D. R. Rolison, J. W. Long, J. C. Lytle, A. E. Fischer, C. P. Rhodes, T. M. McEvoy, M. E. Bourg and A. M. Lubers, *Chem. Soc. Rev.*, 2009, **38**, 226–252.
15 D. Christensen, J. Nijenhuis, J. R. van Ommen and M. O. Coppens, *Ind. Eng. Chem. Res.*, 2008, **47**, 3601–3618.
16 M.-O. Coppens, *Curr. Opin. Chem. Eng.*, 2012, **1**, 281–289.
17 A. Zhakeyev, P. Wang, L. Zhang, W. Shu, H. Wang and J. Xuan, *Adv. Sci.*, 2017, **4**, 1700187.
18 M. Bernardi, N. Ferralis, J. H. Wan, R. Villalon and J. C. Grossman, *Energy Environ. Sci.*, 2012, **5**, 6880–6884.
19 A. Polman and H. A. Atwater, *Nat. Mater.*, 2012, **11**, 174–177.
20 J. H. Atwater, P. Spinelli, E. Kosten, J. Parsons, C. V. Lare, J. V. d. Groep, J. G. d. Abajo, A. Polman and H. A. Atwater, *Appl. Phys. Lett.*, 2011, **99**, 151113.
21 M. Gu, H. Lin and X. Li, *Opt. Lett.*, 2013, **38**, 3627–3630.
22 C.-Y. Lee, A. C. Taylor, A. Nattestad, S. Beirne and G. G. Wallace, *Joule*, 2019, **3**, 1835–1849.
23 M. Gebler, A. J. M. Schoot Uiterkamp and C. Visser, *Energy Policy*, 2014, **74**, 158–167.
24 S. C. Joshi and A. A. Sheikh, *Virtual Phys. Prototyping*, 2015, **10**, 175–185.
25 M. Smith, *Army Sustainment*, 2014, 12–17.
26 P. Wu, J. Wang and X. Wang, *Autom. Constr.*, 2016, **68**, 21–31.
27 N. Tovar, L. Witek, P. Atria, M. Sobieraj, M. Bowers, C. D. Lopez, B. N. Cronstein and P. G. Coelho, *J. Tissue Eng. Regener. Med.*, 2018, **12**, 1986–1999.
28 Q. Yan, H. Dong, J. Su, J. Han, B. Song, Q. Wei and Y. Shi, *Engineering*, 2018, **4**, 729–742.
29 C. Barnatt, *3D Printing*, CreateSpace Independent Publishing Platform, 3rd edn, 2016.
30 I. Gibson, D. W. Rosen, B. Stucker and M. Khorasani, *Additive Manufacturing Technologies*, Springer, 2021.
31 B. C. Gross, J. L. Erkal, S. Y. Lockwood, C. Chen and D. M. Spence, *Anal. Chem.*, 2014, **86**, 3240–3253.
32 A. Waldbaur, H. Rapp, K. Länge and B. E. Rapp, *Anal. Methods*, 2011, **3**, 2681–2716.
33 J. Kim, R. Kumar, A. J. Bandodkar and J. Wang, *Adv. Electron. Mater.*, 2017, **3**, 1600260.
34 X. Zhou and C.-j. Liu, *Adv. Funct. Mater.*, 2017, **27**, 1701134.
35 M. A. S. R. Saadi, A. Maguire, N. T. Pottackal, M. S. H. Thakur, M. M. Ikram, A. J. Hart, P. M. Ajayan and M. M. Rahman, *Adv. Mater.*, 2022, **34**, 2108855.
36 L. Hao, D. Tang, T. Sun, W. Xiong, Z. Feng, K. E. Evans and Y. Li, *Int. J. Precis. Eng. Manuf. – Green Technol.*, 2021, **8**, 665–685.
37 R. D. Farahani, M. Dubé and D. Therriault, *Adv. Mater.*, 2016, **28**, 5794–5821.
38 A. Shen, D. Caldwell, A. W. K. Ma and S. Dardona, *Addit. Manuf.*, 2018, **22**, 343–350.
39 K. Fu, Y. Wang, C. Yan, Y. Yao, Y. Chen, J. Dai, S. Lacey, Y. Wang, J. Wan, T. Li, Z. Wang, Y. Xu and L. Hu, *Adv. Mater.*, 2016, **28**, 2587–2594.
40 Q. Huang and Y. Zhu, *Adv. Mater. Technol.*, 2019, **4**, 1800546.
41 B.-J. de Gans, P. C. Duineveld and U. S. Schubert, *Adv. Mater.*, 2004, **16**, 203–213.
42 K.-S. Kwon, M. K. Rahman, T. H. Phung, S. Hoath, S. Jeong and J. S. Kim, *Flexible Printed Electron.*, 2020, **5**, 043003.
43 J. Chunjiang and C. Guangxue, *J. Part. Sci. Technol.*, 2013, **50**, 160–170.
44 D. Friedmann, A. F. Lee, K. Wilson, R. Jalili and R. A. Caruso, *J. Mater. Chem. A*, 2019, **7**, 10858–10878.
45 P. Yang and H. J. Fan, *Adv. Mater. Technol.*, 2020, **5**, 2000217.
46 B. Nan, F. J. Galindo-Rosales and J. M. F. Ferreira, *Mater. Today*, 2020, **35**, 16–24.

47 S. Yu, M. Xia, J. Sanjayan, L. Yang, J. Xiao and H. Du, *J. Build. Eng.*, 2021, **44**, 102948.
48 Z. Chen, Z. Li, J. Li, C. Liu, C. Lao, Y. Fu, C. Liu, Y. Li, P. Wang and Y. He, *J. Eur. Ceram. Soc.*, 2019, **39**, 661–687.
49 J. Cesarano, R. Segalman and P. Calvert, *Ceram. Ind.*, 1998, **148**, 94–102.
50 C. Zhu, T. Liu, F. Qian, T. Y.-J. Han, E. B. Duoss, J. D. Kuntz, C. M. Spadaccini, M. A. Worsley and Y. Li, *Nano Lett.*, 2016, **16**, 3448–3456.
51 B. A. E. Ben-Arfa, A. S. Neto, I. M. Miranda Salvado, R. C. Pullar and J. M. F. Ferreira, *J. Am. Ceram. Soc.*, 2019, **102**, 1608–1618.
52 A. Shahzad and I. Lazoglu, *Composites, Part B*, 2021, **225**, 109249.
53 M. N. Rahaman and W. Xiao, *Adv. Ceram. Compos.*, 2017, **38**, 235.
54 T. Schlordt, S. Schwanke, F. Keppner, T. Fey, N. Travitzky and P. Greil, *J. Eur. Ceram. Soc.*, 2013, **33**, 3243–3248.
55 J. E. Smay, G. M. Gratson, R. F. Shepherd, J. Cesarano III and J. A. Lewis, *Adv. Mater.*, 2002, **14**, 1279–1283.
56 E. Peng, D. Zhang and J. Ding, *Adv. Mater.*, 2018, **30**, 1802404.
57 L. del-Mazo-Barbara and M.-P. Ginebra, *J. Eur. Ceram. Soc.*, 2021, **41**, 18–33.
58 Y.-Y. Li, L.-T. Li and B. Li, *Mod. Phys. Lett. B*, 2016, **30**, 1650212.
59 L. Yang, X. Zeng and Y. Zhang, *Mater. Lett.*, 2019, **255**, 126564.
60 S. Lamnini, H. Elsayed, Y. Lakhdar, F. Baino, F. Smeacetto and E. Bernardo, *Heliyon*, 2022, **8**, e10651.
61 B. A. Tuttle, J. E. Smay, J. Cesarano, J. A. Voigt, T. W. Scofield, W. R. Olson and J. A. Lewis, *J. Am. Ceram. Soc.*, 2001, **84**, 872–874.
62 M. R. Hartings and Z. Ahmed, *Nat. Rev. Chem.*, 2019, **3**, 305–314.
63 M. Serdeczny, R. Comminal, D. Pedersen and J. Spangenberg, *Presented in Part at the Euspen's 18th International Conference & Exhibition*, 2018.
64 A. Das, C. McIlroy and M. J. Bortner, *Prog. Addit. Manuf.*, 2021, **6**, 3–17.
65 C.-F. Guo, M. Zhang and B. Bhandari, *Computers and Electronics in Agriculture*, 2019, **162**, 397–404.
66 M. P. Serdeczny, R. Comminal, D. B. Pedersen and J. Spangenberg, *Addit. Manuf.*, 2018, **24**, 145–153.
67 R. Comminal, M. P. Serdeczny, D. B. Pedersen and J. Spangenberg, *Addit. Manuf.*, 2018, **20**, 68–76.
68 H. Narei, M. Fatehifar, A. H. Malt, J. Bissell, M. Souri, M. Nasr Esfahani and M. Jabbari, *Polymers*, 2021, **13**, 476.
69 Q. Liu, N. Zhang, W. Wei, X.-j. Hu, Y. Tan, Y. Yu, Y.-J. Deng, C. Bi, L. Zhang and H. Zhang, *J. Food Eng.*, 2020, **275**, 109861.
70 K. Song, D. Zhang, J. Yin and Y. Huang, *Addit. Manuf.*, 2021, **41**, 101963.
71 B. Behdani, M. Senter, L. Mason, M. Leu and J. Park, *J. Manuf. Mater. Process.*, 2020, **4**, 46.
72 E. A. Papon, A. Haque and M. A. R. Sharif, *Rapid Prototyp. J.*, 2021, **27**(3), 518–529.
73 M. M. Cross, *Rheol. Acta*, 1979, **18**, 609–614.
74 V. A. Hackley and C. F. Ferraris, *Guide to rheological nomenclature: measurement in ceramic particulate systems*, Special Publication (NIST SP), 2001.
75 A. Gosset, D. Barreiro-Villaverde, J. C. Becerra Permuy, M. Lema, A. Ares-Pernas and M. J. Abad López, *Polymers*, 2020, **12**, 2885.
76 F. Nikfarjam, Y. Cheny and O. Botella, *Comput. Phys. Commun.*, 2018, **226**, 67–80.
77 P. Antonietti, N. Fadel and M. Verani, *Commun. Appl. Ind. Math.*, 2010, **1**, 1.
78 R. B. Bird, R. C. Armstrong and O. Hassager, *Dynamics of Polymeric Liquids. Vol. 1: Fluid Mechanics*, 1987.
79 G. Yong, *Continuum Mechanics - Progress in Fundamentals and Engineering Applications*, IntechOpen, London, 2012.
80 C. Guo, M. Zhang and S. Devahastin, *J. Food Eng.*, 2020, **286**, 110113.
81 A. Ni, M. N. Prabhakar, I.-H. Suk, J.-K. Park and J.-I. Song, *Mech. Based Des. Struct. Mach.*, 2021, 1–17, DOI: **10.1080/15397734.2021.1919525**.
82 O. Yilmaz, E. Kısasöz, F. Seniha Guner, C. Nart and K. Kirkkopru, *Fibers Polym.*, 2014, **15**, 84–90.
83 V. Hristov and J. Vlachopoulos, *Adv. Polym. Technol.*, 2007, **26**, 100–108.
84 N. D. Gonçalves, O. S. Carneiro and J. M. Nóbrega, *J. Non-Newtonian Fluid Mech.*, 2013, **200**, 103–110.
85 T. J. Coogan and D. O. Kazmer, *Rapid Prototyp. J.*, 2017, **23**, 414–422.
86 B. G. Compton, B. K. Post, C. E. Duty, L. Love and V. Kunc, *Addit. Manuf.*, 2017, **17**, 77–86.
87 T. A. Osswald, J. Puentes and J. Kattinger, *Addit. Manuf.*, 2018, **22**, 51–59.
88 P. Wang, B. Zou, S. Ding, L. Li and C. Huang, *Chin. J. Aeronaut.*, 2021, **34**, 236–246.
89 C. Luo, X. Wang, K. B. Migler and J. E. Seppala, *Addit. Manuf.*, 2020, **32**, 101019.
90 K. Coasey, K. R. Hart, E. Wetzel, D. Edwards and M. E. Mackay, *Addit. Manuf.*, 2020, **33**, 101140.
91 D. A. Edwards and M. E. Mackay, *J. Heat Transfer*, 2020, **142**, 052101.
92 A. D'Amico and A. M. Peterson, *Addit. Manuf.*, 2018, **21**, 422–430.
93 D. D. Phan, Z. R. Swain and M. E. Mackay, *J. Rheol.*, 2018, **62**, 1097–1107.
94 H. Lu, J. Tournet, K. Dastafkan, Y. Liu, Y. H. Ng, S. K. Karuturi, C. Zhao and Z. Yin, *Chem. Rev.*, 2021, **121**, 10271–10366.
95 J. A. Lewis, *Adv. Funct. Mater.*, 2006, **16**, 2193–2204.
96 Y. Li, B. Li and L. Li, *Mod. Phys. Lett. B*, 2014, **28**, 1450051.
97 X. Xu, S. Xiao, H. J. Willy, T. Xiong, R. Borayek, W. Chen, D. Zhang and J. Ding, *Appl. Catal., B*, 2020, **262**, 118307.
98 A. Elkoro and I. Casanova, *3D Printing and Additive Manufacturing*, 2018, **5**, 220–226.
99 C. Xu, T. Liu, W. Guo, Y. Sun, C. Liang, K. Cao, T. Guan, Z. Liang and L. Jiang, *Adv. Eng. Mater.*, 2020, **22**, 1901088.
100 O. H. Laguna, P. F. Lietor, F. J. I. Godino and F. A. Corpas-Iglesias, *Mater. Des.*, 2021, **208**, 109927.

101 M. A. Ávila-López, T. E. Lara-Ceniceros, F. E. Longoria, A. A. Elguezabal, A. Martínez de la Cruz, M. A. Garza-Navarro and J. Bonilla-Cruz, *ACS Appl. Nano Mater.*, 2022, **5**, 11437–11446.
102 E. B. Duoss, M. Twardowski and J. A. Lewis, *Adv. Mater.*, 2007, **19**, 3485–3489.
103 J. Bonilla-Cruz, M. A. Ávila-López, F. E. L. Rodríguez, A. Aguilar-Elguezabal and T. E. Lara-Ceniceros, *J. Eur. Ceram. Soc.*, 2022, **42**, 6033–6039.
104 A. Zaleska, *Recent Pat. Eng.*, 2008, **2**, 157–164.
105 F. Mendez-Arriaga, E. d. l. Calleja, L. Ruiz-Huerta, A. Caballero-Ruiz and R. Almanza, *Mater. Sci. Semicond. Process.*, 2019, **100**, 35–41.
106 Y. Wang, Y. Zhang, S. Wang, Y. Guan and Y. Zhang, *Mater. Today Chem.*, 2021, **22**, 100566.
107 Y. Zhao, Y. Zhao, R. Shi, B. Wang, G. I. N. Waterhouse, L.-Z. Wu, C.-H. Tung and T. Zhang, *Adv. Mater.*, 2019, **31**, 1806482.
108 B. M. Comer and A. J. Medford, *ACS Sustainable Chem. Eng.*, 2018, **6**, 4648–4660.
109 C. Li, T. Wang, Z.-J. Zhao, W. Yang, J.-F. Li, A. Li, Z. Yang, G. A. Ozin and J. Gong, *Angew. Chem., Int. Ed.*, 2018, **57**, 5278–5282.
110 S. Lu, Y. Wang, H. Xiang, H. Lei, B. B. Xu, L. Xing, E. H. Yu and T. X. Liu, *J. Energy Storage*, 2022, **52**, 104764.
111 S. Chandrasekaran, J. Feaster, J. Ynzunza, F. Li, X. Wang, A. J. Nelson and M. A. Worsley, *ACS Mater. Au*, 2022, **2**, 596–601.
112 C. Zhu, Z. Qi, V. A. Beck, M. Luneau, J. Lattimer, W. Chen, M. A. Worsley, J. Ye, E. B. Duoss, C. M. Spadaccini, C. M. Friend and J. Biener, *Sci. Adv.*, 2018, **4**, eaas9459.
113 J. Ahn, Y. S. Park, S. Lee, J. Yang, J. Pyo, J. Lee, G. H. Kim, S. M. Choi and S. K. Seol, *Sci. Rep.*, 2022, **12**, 346.
114 S. M. Thompson, L. Bian, N. Shamsaei and A. Yadollahi, *Addit. Manuf.*, 2015, **8**, 36–62.
115 W. E. Frazier, *J. Mater. Eng. Perform.*, 2014, **23**, 1917–1928.
116 F. C. Walsh, *Pure Appl. Chem.*, 2001, **73**, 1819–1837.
117 M. Krivec, K. Žagar, L. Suhadolnik, M. Čeh and G. Dražić, *ACS Appl. Mater. Interfaces*, 2013, **5**, 9088–9094.
118 A. Yusuf, C. Garlisi and G. Palmisano, *Catal. Today*, 2018, **315**, 79–92.
119 A. Potdar, L. N. Protasova, L. Thomassen and S. Kuhn, *React. Chem. Eng.*, 2017, **2**, 137–148.